AIAA JOURNAL
Vol. 44, No. 1, January 2006

Electromechanically Coupled Zigzag Third-Order Theory for Thermally Loaded Hybrid Piezoelectric Plates

S. Kapuria* and G. G. S. Achary†
Indian Institute of Technology Delhi, New Delhi 110 016, India

An efficient coupled zigzag theory is presented for hybrid piezoelectric plates under thermoelectromechanical loads. The thermal and potential fields are approximated as piecewise linear across sublayers. The deflection is approximated as a combination of a global uniform term across the thickness and local piecewise quadratic variations across sublayers, which explicitly account for the transverse normal strain resulting from thermal and electric fields. The in-plane displacements are approximated as a combination of a third-order global variation across the thickness and a piecewise linear variation across layers. The shear continuity conditions at the layer interfaces and the shear traction-free conditions at the top and bottom are imposed for a general electric field to formulate the theory in terms of five primary displacement variables and potentials. The field equations and boundary conditions are derived from a variational principle. The accuracy of the developed theory is established by direct comparison with three-dimensional exact piezothermoelasticity solutions for simply supported plates under two thermal loads for two very inhomogeneous laminate configurations and different aspect ratios.

I. Introduction

IN laminated composite and sandwich plates, thermal loading causes significant thermal stresses because of the thermal gradient across the thickness and because of the very different thermal properties of the adjacent layers. Embedded or surface-bonded piezoelectric elements can be suitably actuated to reduce undesirable displacements and stresses caused by the thermal environment. Active shape control of thermally loaded structures can be achieved by employing piezoelectric sensor and actuator layers. Development of accurate and efficient two-dimensional models for analysis of hybrid plates, consisting of elastic laminated substrate and piezoelectric layers under a thermal environment, is essential for achieving these objectives. Tauchert et al.[1] have presented a review of the work in thermopiezoelasticity for smart composite structures. The three-dimensional exact piezothermoelasticity solutions[2] of hybrid plates reveal that the material inhomogeneity of the layers causes severe distortion of the lines normal to the midsurface for the moderately thick and thick plates, and these get strained primarily because of transverse thermal and piezoelectric strain. Coupling resulting from direct piezoelectric effect and pyroelectric effect also has a very significant effect on the response under a thermal environment. Classical laminate theory (CLT)[3,4] and first-order shear deformation theory (FSDT)[5,6] have been applied to thermal-stress analysis of hybrid plates without considering electromechanical coupling. Coupled FSDT[7–9] and refined third-order theory (TOT)[10–12] have been developed for analysis of hybrid plates under thermal load that considers direct piezoelectric and pyroelectric coupling effects. These equivalent single layer (ESL) theories, wherein a global expansion of displacements across the thickness is used, are inadequate to account for the distortion in the layers of the lines normal to the midsurface. Discrete layer theories (DLTs)[13] are accurate but the computational cost increases with the number of layers. The shear stress continuity conditions at the layer interfaces are violated in the ESL theories and the DLTs. Kim et al.[14] and Cho and Oh[15] have presented coupled efficient DLTs, also known as zigzag theories, for hybrid shells and plates under thermoelectric load, in which the primary displacement variables are reduced by a priori satisfying the continuity conditions of transverse shear stresses at the layer interfaces and the shear traction-free conditions at the top and bottom surfaces for zero in-plane electric fields. However, these conditions are not satisfied for nonzero in-plane electric field components, which may be induced as a result of piezoelectric coupling or may be applied through segmented piezoelectric actuator layers. Both of these studies consider a global variation of deflection and a linear variation of electric potential across the layers, which is inadequate to capture the nonlinear variation of the electric potential induced by the direct piezoelectric effect.[16] Carrera[17] has recently assessed a variety of ESL theories and DLTs for elastic laminated plates for assumed linear temperature profile across the thickness and an actual temperature profile based on the heat conduction equation. Carrera concluded that 1) the ESL theories often yield inaccurate results even for thin plates, 2) the advanced zigzag theories may work well in thick plates loaded by assumed linear temperature profile but yield inaccurate results for actual temperature profile based on the heat conduction equation, and 3) at least a quadratic variation of deflection in the layers is required to capture even the linear thermal strain in the thickness direction. Kapuria et al.[18] have recently developed an efficient coupled zigzag theory for hybrid solid beams under thermal load that approximates the distribution of thermal and potential fields as piecewise linear across sublayers and accounts directly for the piezoelectric and thermal transverse normal strain in the approximation of deflection. It satisfies the continuity conditions of transverse shear stresses at layer interfaces and the shear traction-free conditions at the top and bottom for the general electric field.

This work presents an efficient coupled third-order zigzag theory for static analysis of hybrid plates under thermoelectric load by extending the zigzag theory of Kapuria[19] to the thermal load case. This work is also an extension of Kapuria and Achary's[20] zigzag theory for elastic laminated plate to hybrid piezoelectric plate. The thermal field is discretized as piecewise linear across the sublayers to approximate the actual thermal profile across the thickness obtained from the three-dimensional thermal heat conduction analysis. The potential field is also similarly approximated as piecewise linear across the sublayers. Both the in-plane and the transverse electric fields are considered. The deflection field is approximated as quadratic in the sublayers, which explicitly accounts for the transverse normal strain induced by the electric and the thermal fields. The in-plane displacements are approximated as a combination of a global third-order variation across the thickness and a piecewise linear variation across the layers. The displacement field is expressed in terms of five primary displacement variables, as in TOT; a set of electric potential variables; and the known thermal field by enforcing exactly the conditions of zero transverse shear stresses at the top and bottom

Received 17 July 2004; revision received 16 July 2005; accepted for publication 26 July 2005.

*Associate Professor, Applied Mechanics Department, Hauz Khas.
†Graduate Student, Applied Mechanics Department, Hauz Khas.

and their continuity at the layer interfaces. The equilibrium equations and boundary conditions are derived using a variational principle. The accuracy of the theory is assessed by direct comparison with the analytical coupled three-dimensional piezothermoelasticity solutions[2,21] for simply supported hybrid plates under thermal load. The results are also compared with the particular case of the present theory with uniform deflection across the thickness (ZIGT) obtained by setting $\alpha_3 = 0$ and $d_{33} = 0$ for all layers and coupled TOT[12] extended to consider sublayer discretization of thermal and potential fields. Comparisons for two thermal loads on a hybrid test plate devised for this study and a hybrid composite plate establish that the present theory yields quite accurate results, far superior to the TOT and the zigzag theory with uniform deflection across thickness.

II. Displacement, Potential, and Thermal Field Approximations

Consider a hybrid plate (Fig. 1) of total thickness h, made of L perfectly bonded layers, some of which can be piezoelectric layers of orthorhombic materials belonging to symmetry class mm2, with poling along z. The plate is subjected to transverse mechanical load and thermal load and has actuation potentials applied to some piezoelectric layers. The kth ply from the bottom has bottom surface at $z = z_{k-1}$. Thus, the bottom and top surfaces are at $z = z_0$ and $z = z_L$. The reference plane $z = 0$ either passes through or is the bottom surface of the k_0th layer. The transverse normal stress σ_z is neglected because the three-dimensional piezothermoelasticity solutions[2,21] have revealed that its contribution to the strain energy is much smaller compared to the contribution of transverse shear stresses and in-plane normal stresses. The linear constitutive equations relating stresses σ,τ and electric displacements D_x, D_y, D_z with strains ε, γ, electric-field components E_x, E_y, E_z, and temperature rise θ are expressed, using the assumption of $\sigma_z \simeq 0$, as

$$\sigma = \bar{Q}\varepsilon - \bar{e}_3^T E_z - \bar{\beta}\theta, \qquad \tau = \hat{Q}\gamma - \hat{e}E$$
$$D = \hat{e}^T\gamma + \hat{\eta}E, \qquad D_z = \bar{e}_3\varepsilon + \bar{\eta}_{33}E_z + \bar{p}_3\theta \tag{1}$$

where, for general angle-ply laminates,

$$\sigma = \begin{bmatrix} \sigma_x \\ \sigma_y \\ \tau_{xy} \end{bmatrix}, \qquad \tau = \begin{bmatrix} \tau_{zx} \\ \tau_{yz} \end{bmatrix}, \qquad D = \begin{bmatrix} D_x \\ D_y \end{bmatrix}$$

$$\varepsilon = \begin{bmatrix} \varepsilon_x \\ \varepsilon_y \\ \gamma_{xy} \end{bmatrix}, \qquad \gamma = \begin{bmatrix} \gamma_{zx} \\ \gamma_{yz} \end{bmatrix}, \qquad E = \begin{bmatrix} E_x \\ E_y \end{bmatrix}$$

$$\bar{Q} = \begin{bmatrix} \bar{Q}_{11} & \bar{Q}_{12} & \bar{Q}_{16} \\ \bar{Q}_{12} & \bar{Q}_{22} & Q_{16} \\ \bar{Q}_{16} & Q_{26} & \bar{Q}_{66} \end{bmatrix}, \qquad \hat{Q} = \begin{bmatrix} \bar{Q}_{55} & \bar{Q}_{45} \\ \bar{Q}_{45} & \bar{Q}_{44} \end{bmatrix}$$

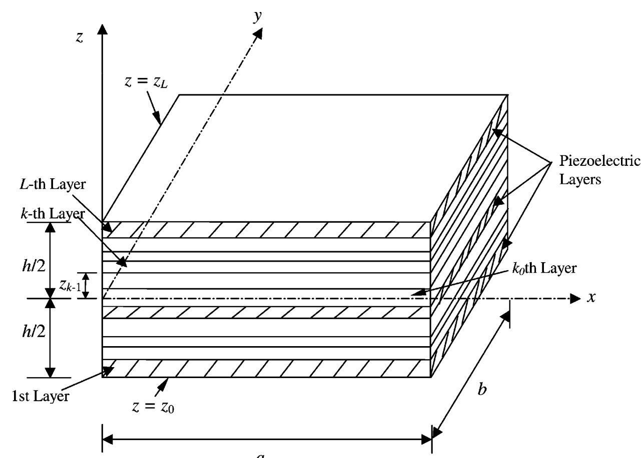

Fig. 1 Geometry of a hybrid plate.

$$\hat{e} = \begin{bmatrix} \bar{e}_{15} & \bar{e}_{14} \\ \bar{e}_{25} & \bar{e}_{24} \end{bmatrix}, \qquad \hat{\eta} = \begin{bmatrix} \bar{\eta}_{11} & \bar{\eta}_{12} \\ \bar{\eta}_{12} & \bar{\eta}_{22} \end{bmatrix}, \qquad \bar{\beta} = \begin{bmatrix} \bar{\beta}_1 \\ \bar{\beta}_2 \\ \bar{\beta}_6 \end{bmatrix}$$
$$\bar{e}_3 = [\bar{e}_{31} \quad \bar{e}_{32} \quad \bar{e}_{36}] \tag{2}$$

$\bar{Q}_{ij}$, $\bar{e}_{ij}$, $\bar{\eta}_{ij}$, and $\bar{\beta}_i$ are the reduced elastic stiffnesses, piezoelectric stress constants, electric permittivities, and stress-temperature coefficients. Let u_x, u_y, and w be the in-plane and transverse displacements and ϕ be the electric potential. Denoting differentiation by a subscript comma, the strain-displacement and the electric field potential relations are

$$\varepsilon_x = u_{x,x}, \qquad \varepsilon_y = u_{y,y}, \qquad \varepsilon_z = w_{,z}$$
$$\gamma_{xy} = u_{x,y} + u_{y,x}, \qquad \gamma_{yz} = u_{y,z} + w_{,y}, \qquad \gamma_{zx} = u_{x,z} + w_{,x}$$
$$E_x = -\phi_{,x}, \qquad E_y = -\phi_{,y}, \qquad E_z = -\phi_{,z} \tag{3}$$

The in-plane electric field components E_x, E_y are not considered as zero, because these may be induced by the piezoelectric coupling or may be applied through actuation of segmented piezoelectric actuators.

The temperature field $\theta(x, y, z)$ for the plate can be solved analytically for some geometries or by the finite-element method. For the present theory, the temperature θ is assumed as piecewise linear between n_θ points z_θ^l, $l = 1, 2, \ldots, n_\theta$, across the thickness. The potential ϕ too is similarly approximated as piecewise linear between n_ϕ points z_ϕ^j, $j = 1, 2, \ldots, n_\phi$, across the thickness:

$$\theta(x, y, z) = \Psi_\theta^l(z)\theta^l(x, y), \qquad \phi(x, y, z) = \Psi_\phi^j(z)\phi^j(x, y) \tag{4}$$

where $\theta^l(x, y) = \theta(x, y, z_\theta^l)$ and $\phi^j(x, y) = \phi(x, y, z_\phi^j)$. $\Psi_\theta^l(z)$ and $\Psi_\phi^j(z)$ are linear interpolation functions, and summation convention is used for indices l, l' (used later) and for indices j, j' (used later). For discretization of θ, each layer is divided into as many sublayers as required for the desired accuracy, depending on the variation of the temperature gradient across its thickness. Similarly, for discretization of ϕ, the piezoelectric layers are divided into sublayers whose number is determined by the required accuracy.

Exact three-dimensional piezothermoelasticity solutions[2] reveal that for moderately thick plates under thermoelectric load, w has significant variation across the layers because of the much greater thermal and electrical contributions to ε_z compared to that of σ_x, σ_y. Most ESL theories and some DLTs ignore this effect and consider w as constant across the thickness. In the present theory, to account for this variation directly without introducing any additional variable, w is approximated by integrating the constitutive equation for ε_z by neglecting elastic compliances S_{13}, S_{23}; that is,

$$\varepsilon_z = w_{,z} = S_{13}\sigma_1 + S_{23}\sigma_2 + d_{33}E_z + \alpha_3\theta \simeq -d_{33}\phi_{,z} + \alpha_3\theta$$
$$\Rightarrow\ w(x, y, z) = w_0(x, y) - \bar{\Psi}_\phi^j(z)\phi^j(x, y) + \bar{\Psi}_\theta^l(z)\theta^l(x, y) \tag{5}$$

where

$$\bar{\Psi}_\phi^j(z) = \int_0^z d_{33}\Psi_{\phi,z}^j(z)\,dz$$

is a piecewise linear function, and

$$\bar{\Psi}_\theta^l(z) = \int_0^z \alpha_3\Psi_\theta^l(z)\,dz$$

is a piecewise quadratic function.

In-plane displacements u_x, u_y are approximated as a combination of third-order variation in z across the laminate thickness and layerwise piecewise linear variation for the kth layer:

$$u(x, y, z) = u_k(x, y) - zw_{0_d}(x, y) + z\psi_k(x, y)$$
$$+ z^2\xi(x, y) + z^3\eta(x, y) \tag{6}$$

where

$$u = \begin{bmatrix} u_x \\ u_y \end{bmatrix}, \qquad w_{0_d} = \begin{bmatrix} w_{0,x} \\ w_{0,y} \end{bmatrix}, \qquad u_k = \begin{bmatrix} u_{k_x} \\ u_{k_y} \end{bmatrix}$$
$$\psi_k = \begin{bmatrix} \psi_{k_x} \\ \psi_{k_y} \end{bmatrix}, \qquad \xi = \begin{bmatrix} \xi_x \\ \xi_y \end{bmatrix}, \qquad \eta = \begin{bmatrix} \eta_x \\ \eta_y \end{bmatrix} \tag{7}$$

u_k is the translation, and ψ_k is related to the shear rotation of the kth layer.

Substituting u_x, u_y, and w from Eqs. (6) and (5), and ϕ from Eq. (4), into Eqs. (3) and using Eq. (1) yields the transverse shear stresses τ yields

$$\tau = \hat{Q}^k\left(\psi_k + 2z\xi + 3z^2\eta\right) + \left[\hat{e}^k\Psi^j_\phi(z) - \hat{Q}^k\bar{\Psi}^j_\phi(z)\right]\phi^j_d + \hat{Q}^k\bar{\Psi}^l_\theta(z)\theta^l_d \tag{8}$$

where $\phi^j_d = [\phi^j_{,x}\ \ \phi^j_{,y}]^T$ and $\theta^l_d = [\theta^l_{,x}\ \ \theta^l_{,y}]^T$. Let, at the midplane through the k_0th layer, $u_0(x, y) = u_{k_0}(x, y) = u(x, y, 0)$ and $\psi_0(x, y) = \psi_{k_0}(x, y)$. The $(4L+4)$ unknowns u_k, ψ_k, ξ, η for the L-layered laminate are reduced to only four unknowns u_0 and ψ_0 by enforcing the $2(L-1)$ conditions each for the continuity of τ and u at the layer interfaces and the four shear traction-free conditions $\tau = 0$ at $z = z_0, z_L$. To do so, the continuity condition of τ at interface $z = z_{i-1}$ between layers i and $i-1$ is expressed in a recursive form using Eq. (8):

$$\begin{aligned}
&\hat{Q}^i\left(\psi_i + 2z_i\xi + 3z_i^2\eta\right) + \left[\hat{e}^i\Psi^j_\phi(z_i) - \hat{Q}^i\bar{\Psi}^j_\phi(z_i)\right]\phi^j_d + \hat{Q}^i\bar{\Psi}^l_\theta(z_i)\theta^l_d \\
&\quad = \hat{Q}^{i-1}\left(\psi_{i-1} + 2z_{i-1}\xi + 3z_{i-1}^2\eta\right) + \left[\hat{e}^{i-1}\Psi^j_\phi(z_{i-1}) \right.\\
&\quad \left. - \hat{Q}^{i-1}\bar{\Psi}^j_\phi(z_{i-1})\right]\phi^j_d + \hat{Q}^{i-1}\bar{\Psi}^l_\theta(z_{i-1})\theta^l_d + 2\hat{Q}^i(z_i - z_{i-1})\xi \\
&\quad + 3\hat{Q}^i\left(z_i^2 - z_{i-1}^2\right)\eta + \left\{\hat{e}^i\left[\Psi^j_\phi(z_i) - \Psi^j_\phi(z_{i-1})\right]\right. \\
&\quad \left. - \hat{Q}^i\left[\bar{\Psi}^j_\phi(z_i) - \bar{\Psi}^j_\phi(z_{i-1})\right]\right\}\phi^j_d + \hat{Q}^i\left[\bar{\Psi}^l_\theta(z_i) - \bar{\Psi}^l_\theta(z_{i-1})\right]\theta^l_d
\end{aligned} \tag{9}$$

Using the condition $\tau(x, y, z_0) = 0$ in Eq. (8) for $k = 1$ and adding Eq. (9) from $i = 2$ to k yields the following expression for τ^k at the kth interface at $z = z_k$ for $k = 2, \ldots, L$:

$$\begin{aligned}
\tau^k &= \hat{Q}^k\left(\psi_k + 2z_k\xi + 3z_k^2\eta\right) + \left[\hat{e}^k\Psi^j_\phi(z_k) - \hat{Q}^k\bar{\Psi}^j_\phi(z_k)\right]\phi^j_d \\
&\quad + \hat{Q}^k\bar{\Psi}^l_\theta(z_k)\theta^l_d = 2C^k_1\xi + 6C^k_2\eta + C^k_{3j}\phi^j_d + C^k_{4l}\theta^l_d
\end{aligned} \tag{10}$$

where

$$C^k_1 = \sum_{i=1}^{k}\hat{Q}^i(z_i - z_{i-1}), \qquad C^k_2 = \sum_{i=1}^{k}\hat{Q}^i\left(z_i^2 - z_{i-1}^2\right)/2$$
$$C^k_{3j} = \sum_{i=1}^{k}\left\{\hat{e}^i\left[\Psi^j_\phi(z_i) - \Psi^j_\phi(z_{i-1})\right] - \hat{Q}^i\left[\bar{\Psi}^j_\phi(z_i) - \bar{\Psi}^j_\phi(z_{i-1})\right]\right\}$$
$$C^k_{4l} = \sum_{i=1}^{k}\hat{Q}^i\left[\bar{\Psi}^l_\theta(z_i) - \bar{\Psi}^l_\theta(z_{i-1})\right]$$

By solving the equations obtained by imposing the condition $\tau_{zx}(x, y, z_L) = \tau^L = 0$ in Eq. (10) for $k = L$ and the condition $\tau_{zx}(x, y, z_0) = 0$ in Eq. (8) for $k = 1$, the unknown functions ξ, η are obtained as

$$\xi = R_3\psi_1 + R^j_5\phi^j_d + R^l_7\theta^l_d, \qquad \eta = R_4\psi_1 + R^j_6\phi^j_d + R^l_8\theta^l_d \tag{11}$$

where

$$\Delta = 4z_0^2C^L_1 - 8z_0C^L_2, \qquad R_3 = 4\Delta^{-1}C^L_2$$
$$R_4 = -4\Delta^{-1}C^L_1/3$$
$$R^j_5 = -\Delta^{-1}\left(2z_0^2C^L_{3j} + 4C^L_2C^j_5\right)$$
$$R^l_7 = -\Delta^{-1}\left(2z_0^2C^L_{4l} + 4C^L_2C^l_6\right)$$
$$R^j_6 = \Delta^{-1}\left(4z_0C^L_{3j} + 4C^L_1C^j_5\right)/3$$
$$R^l_8 = \Delta^{-1}\left(4z_0C^L_{4l} + 4C^L_1C^l_6\right)/3$$
$$C^j_5 = \bar{\Psi}^j_\phi(z_0)I_2 - (\hat{Q}^1)^{-1}\hat{e}^1\Psi^j_\phi(z_0)$$
$$C^l_6 = -\bar{\Psi}^l_\theta(z_0)I_2 \tag{12}$$

I_2 is a 2×2 identity matrix. Substituting ξ, η from Eq. (11) into Eq. (10) yields

$$\psi_k = R^k_2\psi_1 + R^k_{j1}\phi^j_d + R^k_{l2}\theta^l_d \tag{13}$$

where

$$R^k_2 = a^k_1R_3 + a^k_2R_4$$
$$R^k_{j1} = a^k_1R^j_5 + a^k_2R^j_6 + (\hat{Q}^k)^{-1}\left[C^k_{3j} - \hat{e}^k\Psi^j_\phi(z_k)\right] + \bar{\Psi}^j_\phi(z_k)I_2$$
$$R^k_{l2} = a^k_1R^l_7 + a^k_2R^l_8 + (\hat{Q}^k)^{-1}C^k_{4l} - \bar{\Psi}^l_\theta(z_k)I_2$$
$$a^k_1 = 2\left[(\hat{Q}^k)^{-1}C^k_1 - z_kI_2\right], \qquad a^k_2 = 3\left[2(\hat{Q}^k)^{-1}C^k_2 - z_k^2I_2\right] \tag{14}$$

Using Eq. (6), continuity of u between layers i and $i-1 \Rightarrow u_i + z_{i-1}\psi_i = u_{i-1} + z_{i-1}\psi_{i-1}$, and using Eq. (13), u_k can be expressed in terms of u_1 and ψ_1 as

$$u_k = u_1 + \bar{R}^k_2\psi_1 + \bar{R}^k_{j1}\phi^j_d + \bar{R}^k_{l2}\theta^l_d \tag{15}$$

where

$$\bar{R}^k_2 = \sum_{i=2}^{k}z_{i-1}\left(R^{i-1}_2 - R^i_2\right), \qquad \bar{R}^k_{j1} = \sum_{i=2}^{k}z_{i-1}\left(R^{i-1}_{j1} - R^i_{j1}\right)$$
$$\bar{R}^k_{l2} = \sum_{i=2}^{k}z_{i-1}\left(R^{i-1}_{l2} - R^i_{l2}\right)$$

By substituting the expressions of u_k, ψ_k, ζ, η from Eqs. (11), (13), and (15) in Eq. (6) and expressing u_1 and ψ_1 in terms of the midplane displacement variables $u_0(x, y)$ and $\psi_0(x, y)$, u is finally obtained as

$$\begin{aligned}
u(x, y, z) &= u_0(x, y) - zw_{0_d}(x, y) + R^k(z)\psi_0(x, y) \\
&\quad + R^{kj}(z)\phi^j_d(x, y) + \bar{R}^{kl}(z)\theta^l_d(x, y)
\end{aligned} \tag{16}$$

where

$$R^k(z) = \hat{R}^k_1 + z\hat{R}^k_2 + z^2\hat{R}_3 + z^3\hat{R}_4$$
$$\left(\hat{R}^k_1, \hat{R}^k_2, \hat{R}_3, \hat{R}_4\right) = \left(\bar{R}^k_2 - \bar{R}^{k_0}_2, R^k_2, R_3, R_4\right)\left(R^{k_0}_2\right)^{-1}$$
$$R^{kj}(z) = \hat{R}^{kj}_1 + z\hat{R}^k_{j1} + z^2\hat{R}^j_5 + z^3\hat{R}^j_6$$
$$\bar{R}^{kl}(z) = \hat{R}^{kl}_2 + z\hat{R}^k_{l2} + z^2\hat{R}^l_7 + z^3\hat{R}^l_8$$
$$\hat{R}^{kj}_1 = \bar{R}^k_{j1} - \bar{R}^{k_0}_{j1} - \hat{R}^k_1R^{k_0}_{j1}, \qquad \hat{R}^k_{j1} = R^k_{j1} - \hat{R}^k_2R^{k_0}_{j1}$$
$$\hat{R}^j_5 = R^j_5 - \hat{R}_3R^{k_0}_{j1}, \qquad \hat{R}^j_6 = R^j_6 - \hat{R}_4R^{k_0}_{j1}$$
$$\hat{R}^{kl}_2 = \bar{R}^k_{l2} - \bar{R}^{k_0}_{l2} - \hat{R}^k_1R^{k_0}_{l2}, \qquad \hat{R}^k_{l2} = R^k_{l2} - \hat{R}^k_2R^{k_0}_{l2}$$
$$\hat{R}^l_7 = R^l_7 - \hat{R}_3R^{k_0}_{l2}, \qquad \hat{R}^l_8 = R^l_8 - \hat{R}_4R^{k_0}_{l2} \tag{17}$$

Thus, ϕ, w, u are expressed in terms of the five primary mechanical displacement variables u_{0_x}, u_{0_y}, w_0, ψ_{0_x}, ψ_{0_y}, and ϕ^j by Eqs. (4), (5), and (16).

III. Electromechanically Coupled Field Equations

The variational principle for the piezoelectric medium[22] can be expressed, using the notation

$$\langle\ldots\rangle = \sum_{k=1}^{L}\int_{z^+_{k-1}}^{z^-_k}(\ldots)\,dz$$

for integration across the thickness, as

$$\int_A \Big[\langle \sigma_x\delta\varepsilon_x + \sigma_y\delta\varepsilon_y + \tau_{xy}\delta\gamma_{xy} + \tau_{yz}\delta\gamma_{yz} + \tau_{zx}\delta\gamma_{zx} + D_x\delta\phi_{,x} + D_y\delta\phi_{,y} + D_z\delta\phi_{,z}\rangle - p_z^1\delta w(x,y,z_0) - p_z^2\delta w(x,y,z_L) + D_z(x,y,z_0)\delta\phi^1 - D_z(x,y,z_L)\delta\phi^{n_\phi} - q_{j_i}\delta\phi^{j_i}\Big]dA - \int_{\Gamma_L}\langle \sigma_n\delta u_n + \tau_{ns}\delta u_s + \tau_{nz}\delta w + D_n\delta\phi\rangle ds = 0 \tag{18}$$

$\forall\delta u_0, \delta w_0, \delta\psi_0, \delta\phi^j$, where A denotes the midplane surface area of the plate and Γ_L is the boundary curve of the midplane of the plate with normal n and tangent s. Variables p_z^1, p_z^2 are the forces per unit area applied on the bottom and top surfaces of the plate in direction z. Variable q_{j_i} is the the extraneous surface charge density on the interface $z = z_\phi^{j_i}$, where ϕ^{j_i} is prescribed. The total number of such prescribed potentials is $\bar{n}_\phi$. This variational equation is expressed in terms of $\delta u_0, \delta w_0, \delta\psi_0, \delta\phi^j$, and stress and electric displacement resultants to yield field equations and boundary conditions. The stress resultants $N = [N_x\ N_y\ N_{xy}]^T$, $M = [M_x\ M_y\ M_{xy}]^T$, $P = [P_x\ P_{yx}\ P_{xy}\ P_y]^T$, $S^j = [S_x^j\ S_{yx}^j\ S_{xy}^j\ S_y^j]^T$, $Q = [Q_x\ Q_y]^T$, $\bar{Q}^j = [\bar{Q}_x^j\ \bar{Q}_y^j]^T$, $V = [V_x\ V_y]^T$, $V_\phi^j = [V_{\phi_x}^j\ V_{\phi_y}^j]^T$, and the electric displacement resultants $H^j = [H_x^j\ H_y^j]^T$, G^j are defined by

$$F_1 = \begin{bmatrix} N^T & M^T & P^T & S^{j\,T}\end{bmatrix}^T = \big[\langle f_3^T\sigma\rangle\big]$$
$$F_2 = \begin{bmatrix} Q_x & Q_y & \bar{Q}_x^j & \bar{Q}_y^j\end{bmatrix}^T = \big[\langle f_4^T\tau\rangle\big]$$
$$V = \langle\tau\rangle, \qquad V_\phi^j = \langle\bar{\Psi}_\phi^j\tau\rangle$$
$$H^j = \langle\Psi_\phi^j(z)D\rangle, \qquad G^j = \langle\Psi_{\phi,z}^j(z)D_z\rangle \tag{19}$$

where $f_3 = [I_3\ \ zI_3\ \ \Phi^k\ \ \Phi^{kj}]$, $f_4 = [R_{,z}^k\ \ R_{,z}^{kj} - \bar{\Psi}_\phi^j(z)I_2]$, I_3 is a 3×3 identity matrix, and

$$\Phi^k = \begin{bmatrix} R_{11}^k & 0 & R_{12}^k & 0 \\ 0 & R_{21}^k & 0 & R_{22}^k \\ R_{21}^k & R_{11}^k & R_{22}^k & R_{12}^k \end{bmatrix}$$
$$\Phi^{kj} = \begin{bmatrix} R_{11}^{kj} & 0 & R_{12}^{kj} & 0 \\ 0 & R_{21}^{kj} & 0 & R_{22}^{kj} \\ R_{21}^{kj} & R_{11}^{kj} & R_{22}^{kj} & R_{12}^{kj} \end{bmatrix} \tag{20}$$

It can be shown that elements of R^k, R^{kj}, N, M, P, S^j transform as second-order tensors, and elements of V, V_ϕ^j, Q, $\bar{Q}^j$, H^j transform as vectors for the coplanar axes x, y and n, s. The resultants F_1, F_2, H^j, G^j can be expressed in terms of the displacement and potential variables by substituting the expressions of σ, τ, D, D_z from Eq. (1) into Eq. (19) and using Eqs. (3–5) and (16):

$$F_1 = A\bar{\varepsilon}_1 + \beta^{j'}\phi^{j'} + A^l\theta_{dd}^l - \gamma^l\theta^l$$
$$F_2 = \bar{A}\bar{\varepsilon}_2 + \bar{\beta}^{j'}\phi_d^{j'} + \bar{A}^l\theta_d^l$$
$$H^j = \bar{\beta}^{j^T}\bar{\varepsilon}_2 - \bar{E}^{jj'}\phi_d^{j'} + \bar{\beta}^{jl}\theta_d^l$$
$$G^j = \beta^{j^T}\bar{\varepsilon}_1 - E^{jj'}\phi^{j'} + \beta^{jl}\theta_{dd}^l + \gamma^{jl}\theta^l \tag{21}$$

where

$$\bar{\varepsilon}_1 = \begin{bmatrix} u_{0_x,x} & u_{0_y,y} & u_{0_x,y}+u_{0_y,x} & -w_{0,xx} & -w_{0,yy} & -2w_{0,xy} & \psi_{0_x,x} & \psi_{0_x,y} & \psi_{0_y,x} & \psi_{0_y,y} & \phi_{,xx}^j & \phi_{,xy}^j & \phi_{,yx}^j & \phi_{,yy}^j \end{bmatrix}^T$$
$$\bar{\varepsilon}_2 = \begin{bmatrix}\psi_{0_x} & \psi_{0_y} & \phi_{,x}^j & \phi_{,y}^j\end{bmatrix}^T, \qquad [A, A^l] = \langle f_3^T(z)\bar{Q}\big[f_3(z), \bar{\Phi}^{kl}(z)\big]\rangle, \qquad [\bar{A}, \bar{A}^l] = \langle f_4^T(z)\hat{Q}\big[f_4(z), \bar{\Gamma}^{kl}(z)\big]\rangle$$
$$\beta^{j'} = \langle f_3^T(z)\bar{e}_3^T\Psi_{\phi,z}^{j'}(z)\rangle, \qquad \bar{\beta}^{j'} = \langle f_4^T(z)\hat{e}\Psi_\phi^{j'}(z)\rangle, \qquad E^{jj'} = \langle\bar{\eta}_{33}\Psi_{\phi,z}^j(z)\Psi_{\phi,z}^{j'}(z)\rangle, \qquad \bar{E}^{jj'} = \langle\hat{\eta}\Psi_\phi^j(z)\Psi_\phi^{j'}(z)\rangle$$
$$\bar{\Gamma}^{kl}(z) = \bar{R}_{,z}^{kl}(z) + \bar{\Psi}_\theta^l(z)I_2, \qquad \gamma^l = \langle\bar{f}_3^T(z)\bar{\beta}\Psi_\theta^l(z)\rangle, \qquad \gamma^{jl} = \langle\bar{p}_3\Psi_{\phi,z}^j(z)\Psi_\theta^l(z)\rangle$$
$$\beta^{jl} = \langle\Psi_{\phi,z}^j(z)\bar{e}_3\bar{\Phi}^{kl}(z)\rangle, \qquad \bar{\beta}^{jl} = \langle\Psi_\phi^j(z)\hat{e}^T\bar{\Gamma}^{kl}(z)\rangle \tag{22}$$

$$A = \begin{bmatrix} A_{11} & A_{12} & \dots & A_{1,10} & A_{1,11}^{j'} & A_{1,12}^{j'} & A_{1,13}^{j'} & A_{1,14}^{j'} \\ A_{21} & A_{22} & \dots & A_{2,10} & A_{2,11}^{j'} & A_{2,12}^{j'} & A_{2,13}^{j'} & A_{2,14}^{j'} \\ \vdots & \vdots & \vdots & \vdots & \vdots & \vdots & \vdots & \vdots \\ A_{10,1} & A_{10,2} & \dots & A_{10,10} & A_{10,11}^{j'} & A_{10,12}^{j'} & A_{10,13}^{j'} & A_{10,14}^{j'} \\ A_{11,1}^j & A_{11,2}^j & \dots & A_{11,10}^j & A_{11,11}^{jj'} & A_{11,12}^{jj'} & A_{11,13}^{jj'} & A_{11,14}^{jj'} \\ A_{12,1}^j & A_{12,2}^j & \dots & A_{12,10}^j & A_{12,11}^{jj'} & A_{12,12}^{jj'} & A_{12,13}^{jj'} & A_{12,14}^{jj'} \\ A_{13,1}^j & A_{13,2}^j & \dots & A_{13,10}^j & A_{13,11}^{jj'} & A_{13,12}^{jj'} & A_{13,13}^{jj'} & A_{13,14}^{jj'} \\ A_{14,1}^j & A_{14,2}^j & \dots & A_{14,10}^j & A_{14,11}^{jj'} & A_{14,12}^{jj'} & A_{14,13}^{jj'} & A_{14,14}^{jj'} \end{bmatrix} = A^T, \quad A^l = \begin{bmatrix} A_{11}^l & A_{12}^l & A_{13}^l & A_{14}^l \\ A_{21}^l & A_{22}^l & A_{23}^l & A_{24}^l \\ \vdots & \vdots & \vdots & \\ A_{10,1}^l & A_{10,2}^l & A_{10,3}^l & A_{10,4}^l \\ A_{11,1}^{jl} & A_{11,2}^{jl} & A_{11,3}^{jl} & A_{11,4}^{jl} \\ A_{12,1}^{jl} & A_{12,2}^{jl} & A_{12,3}^{jl} & A_{12,4}^{jl} \\ A_{13,1}^{jl} & A_{13,2}^{jl} & A_{13,3}^{jl} & A_{13,4}^{jl} \\ A_{14,1}^{jl} & A_{14,2}^{jl} & A_{14,3}^{jl} & A_{14,4}^{jl} \end{bmatrix}, \quad \beta^{j'} = \begin{bmatrix} \beta_1^{j'} \\ \beta_2^{j'} \\ \vdots \\ \beta_{10}^{j'} \\ \beta_{11}^{jj'} \\ \beta_{12}^{jj'} \\ \beta_{13}^{jj'} \\ \beta_{14}^{jj'} \end{bmatrix}$$

$$\gamma^l = \begin{bmatrix} \gamma_1^l \\ \gamma_2^l \\ \vdots \\ \gamma_{10}^l \\ \gamma_{11}^{jl} \\ \gamma_{12}^{jl} \\ \gamma_{13}^{jl} \\ \gamma_{14}^{jl} \end{bmatrix}, \quad \bar{A} = \begin{bmatrix} \bar{A}_{11} & \bar{A}_{12} & \bar{A}_{13}^{j'} & \bar{A}_{14}^{j'} \\ \bar{A}_{21} & \bar{A}_{22} & \bar{A}_{23}^{j'} & \bar{A}_{24}^{j'} \\ \bar{A}_{31}^j & \bar{A}_{32}^j & \bar{A}_{33}^{jj'} & \bar{A}_{34}^{jj'} \\ \bar{A}_{41}^j & \bar{A}_{42}^j & \bar{A}_{43}^{jj'} & \bar{A}_{44}^{jj'} \end{bmatrix} = \bar{A}^T, \quad \bar{A}^l = \begin{bmatrix} \bar{A}_{11}^l & \bar{A}_{12}^l \\ \bar{A}_{21}^l & \bar{A}_{22}^l \\ \bar{A}_{31}^{jl} & \bar{A}_{32}^{jl} \\ \bar{A}_{41}^{jl} & \bar{A}_{42}^{jl} \end{bmatrix}, \quad \bar{\beta}^{j'} = \begin{bmatrix} \bar{\beta}_{11}^{j'} & \bar{\beta}_{12}^{j'} \\ \bar{\beta}_{21}^{j'} & \bar{\beta}_{22}^{j'} \\ \bar{\beta}_{31}^{jj'} & \bar{\beta}_{32}^{jj'} \\ \bar{\beta}_{41}^{jj'} & \bar{\beta}_{42}^{jj'} \end{bmatrix}$$

$$\bar{\beta}^{jl} = \begin{bmatrix} \bar{\beta}_{11}^{jl} & \bar{\beta}_{12}^{jl} \\ \bar{\beta}_{21}^{jl} & \bar{\beta}_{22}^{jl} \end{bmatrix}, \qquad \bar{E}^{jj'} = \begin{bmatrix} \bar{E}_{11}^{jj'} & \bar{E}_{12}^{jj'} \\ \bar{E}_{21}^{jj'} & \bar{E}_{22}^{jj'} \end{bmatrix}, \qquad \beta^{jl} = \begin{bmatrix}\beta_1^{jl} & \beta_2^{jl} & \beta_3^{jl} & \beta_4^{jl}\end{bmatrix} \tag{23}$$

Using expressions of w, ϕ, u from Eqs. (4), (5), and (16) and using Eq. (19), the area integral in Eq. (18) is expressed in terms of $\delta u_{0_x}, \delta u_{0_y}, \delta w_0, \delta\psi_{0_x}, \delta\psi_{0_y}, \delta\phi^j$ by using Green's theorem if required, and the terms involving $\delta u_{0_x}, \delta u_{0_y}, \delta\psi_{0_x}, \delta\psi_{0_y}, \delta w_{0,x}, \delta w_{0,y}, \delta\phi^j_{,x}, \delta\phi^j_{,y}$ in the integrand of Γ_L are expressed in terms of components n, s. Thus, Eq. (18) yields coupled field equations consisting of five equations of equilibrium and n_ϕ equations for electric potentials:

$$
\begin{aligned}
&-N_{x,x} - N_{xy,y} = 0, \qquad -N_{xy,x} - N_{y,y} = 0\\
&-M_{x,xx} - 2M_{xy,xy} - M_{y,yy} - F_3 = 0\\
&-P_{x,x} - P_{yx,y} + Q_x = 0, \qquad -P_{xy,x} - P_{y,y} + Q_y = 0\\
&-\bar{Q}^j_{x,x} - \bar{Q}^j_{y,y} + S^j_{x,xx} + S^j_{xy,xy} + S^j_{yx,xy} + S^j_{y,yy} - H^j_{x,x}\\
&\quad -H^j_{y,y} + G^j - F^j_6 = 0, \qquad j = 1, 2, \ldots, n_\phi
\end{aligned} \tag{24}
$$

where the mechanical load $F_3 = p^1_z + p^2_z$ and the electrical loads $F^j_6 = D_z(x, y, z_L)\delta_{jn_\phi} - D_z(x, y, z_0)\delta_{j1} + q_{j_i}\delta_{jj_i}$. The boundary conditions on Γ_L are the prescribed values of one of the factors of each of the following products:

$$
\begin{aligned}
&u_{0_n} N_n, \qquad u_{0_s} N_{ns}, \qquad w_0(V_n + M_{ns,s}), \qquad w_{0,n} M_n\\
&\psi_{0_n} P_n, \qquad \psi_{0_s} P_{ns}, \qquad \phi^j_{,n} S^j_n, \qquad \phi^j\left[H^j_n - V^j_{\phi_n} - S^j_{ns,s}\right]
\end{aligned}
$$

and at corners s_i

$$
w_0(s_i)\Delta M_{ns}(s_i), \qquad \phi^j(s_i)\Delta S^j_{ns}(s_i) \tag{25}
$$

with

$$
\begin{aligned}
V_n &= (M_{x,x} + M_{xy,y})n_x + (M_{xy,x} + M_{y,y})n_y\\
V^j_{\phi_n} &= \left(S^j_{x,x} + S^j_{yx,y}\right)n_x + \left(S^j_{y,y} + S^j_{xy,x}\right)n_y - \bar{Q}^j_x n_x - \bar{Q}^j_y n_y
\end{aligned}
$$

Substituting the expressions of the resultants from Eqs. (21) into Eqs. (24) yields the following coupled electromechanical equations in terms of the primary displacement and potential field variables $\bar{U}$:

$$
L\bar{U} = \bar{P} \tag{26}
$$

where

$$
\begin{aligned}
\bar{U} &= \begin{bmatrix} u_{0_x} & u_{0_y} & w_0 & \psi_{0_x} & \psi_{0_y} & \phi^1 & \phi^2 & \cdots & \phi^{n_\phi} \end{bmatrix}^T\\
\bar{P} &= \begin{bmatrix} P_1 & P_2 & P_3 & P_4 & P_5 & P^1_6 & P^2_6 & \cdots & P^{n_\phi}_6 \end{bmatrix}^T
\end{aligned} \tag{27}
$$

L is a symmetric matrix of linear differential operators in x and y. For cross-ply plates, because $\bar{Q}_{45} = 0$, $Q_{16} = \bar{Q}_{26} = 0$, $\bar{e}_{14} = \bar{e}_{25} = 0$, $\bar{\beta}_6 = 0$, $\bar{\eta}_{12} = 0$, and $\bar{e}_{36} = 0$; taking into account the corresponding zero elements of A, A^l, $\bar{A}$, $\bar{A}^l$, β^j, $\bar{\beta}^j$, β^{jl}, $\bar{\beta}^{jl}$, $\bar{E}^{jj'}$, γ^l, γ^{jl}, the elements of L are

$$
\begin{aligned}
L_{11} &= -A_{11}()_{,xx} - A_{33}()_{,yy}, \qquad L_{12} = -(A_{12} + A_{33})()_{,xy}\\
L_{13} &= A_{14}()_{,xxx} + (A_{15} + 2A_{36})()_{,xyy}\\
L_{14} &= -A_{17}()_{,xx} - A_{38}()_{,yy}\\
L_{15} &= -(A_{1,10} + A_{39})()_{,xy}, \qquad L_{22} = -A_{22}()_{,yy} - A_{33}()_{,xx}\\
L_{1,5+j'} &= -A^{j'}_{1,11}()_{,xxx} - \left(A^{j'}_{3,12} + A^{j'}_{3,13} + A^{j'}_{1,14}\right)()_{,xyy} - \beta^{j'}_1()_{,x}\\
L_{23} &= (A_{24} + 2A_{36})()_{,xxy} + A_{25}()_{,yyy}\\
L_{24} &= -(A_{27} + A_{38})()_{,xy}\\
L_{2,5+j'} &= -\left(A^{j'}_{2,11} + A^{j'}_{3,12} + A^{j'}_{3,13}\right)()_{,xxy} - A^{j'}_{2,14}()_{,yyy} - \beta^{j'}_2()_{,y}\\
L_{25} &= -A_{39}()_{,xx} - A_{2,10}()_{,yy}\\
L_{33} &= -A_{44}()_{,xxxx} - (A_{45} + A_{54} + 4A_{66})()_{,xxyy} - A_{55}()_{,yyyy}\\
L_{34} &= A_{47}()_{,xxx} + (A_{57} + 2A_{68})()_{,xyy}\\
L_{35} &= (A_{4,10} + 2A_{69})()_{,xxy} + A_{5,10}()_{,yyy}\\
L_{3,5+j'} &= A^{j'}_{4,11}()_{,xxxx} + \left(A^{j'}_{4,14} + 2A^{j'}_{6,12} + 2A^{j'}_{6,13}\right.\\
&\quad \left. + A^{j'}_{5,11}\right)()_{,xxyy} + A^{j'}_{5,14}()_{,yyyy} + \beta^{j'}_4()_{,xx} + \beta^{j'}_5()_{,yy}\\
L_{44} &= \bar{A}_{11} - A_{77}()_{,xx} - A_{88}()_{,yy}, \qquad L_{45} = -(A_{7,10} + A_{89})()_{,xy}\\
L_{4,5+j'} &= -A^{j'}_{7,11}()_{,xxx} - \left(A^{j'}_{7,14} + A^{j'}_{8,12} + A^{j'}_{8,13}\right)()_{,xyy}\\
&\quad + \left(\bar{A}^{j'}_{13} + \bar{\beta}^{j'}_{11} - \beta^{j'}_7\right)()_{,x}\\
L_{55} &= \bar{A}_{22} - A_{9,9}()_{,xx} - A_{10,10}()_{,yy}\\
L_{5,5+j'} &= -\left(A^{j'}_{9,12} + A^{j'}_{9,13} + A^{j'}_{10,11}\right)()_{,xxy} - A^{j'}_{10,14}()_{,yyy}\\
&\quad + \left(\bar{A}^{j'}_{24} + \bar{\beta}^{j'}_{22} - \beta^{j'}_{10}\right)()_{,y}\\
L_{5+j,5+j'} &= -A^{jj'}_{11,11}()_{,xxxx} - \left(A^{jj'}_{11,14} + A^{jj'}_{12,12} + A^{jj'}_{12,13} + A^{jj'}_{13,12}\right.\\
&\quad \left. + A^{jj'}_{13,13} + A^{jj'}_{14,11}\right)()_{,xxyy}\\
&\quad - A^{jj'}_{14,14}()_{,yyyy} + \left[\bar{A}^{jj'}_{33} - \beta^{jj'}_{11} - \beta^{j'j}_{11} + \bar{\beta}^{jj'}_{31} + \bar{\beta}^{j'j}_{31} - \bar{E}^{jj'}_{11}\right]()_{,xx}\\
&\quad + \left[\bar{A}^{jj'}_{44} - \beta^{jj'}_{14} - \beta^{j'j}_{14} + \bar{\beta}^{jj'}_{42} + \bar{\beta}^{j'j}_{42} - \bar{E}^{jj'}_{22}\right]()_{,yy} + E^{jj'}
\end{aligned} \tag{28}
$$

where $j, j' = 1, \ldots, n_\phi$. The elements of load vector P are

$$
\begin{aligned}
P_1 &= A^l_{11}\theta^l_{,xxx} + \left(A^l_{14} + A^l_{32} + A^l_{33}\right)\theta^l_{,xyy} - \gamma^l_1\theta^l_{,x}\\
P_2 &= \left(A^l_{21} + A^l_{32} + A^l_{33}\right)\theta^l_{,xxy} + A^l_{24}\theta^l_{,yyy} - \gamma^l_2\theta^l_{,y}\\
P_3 &= -F_3 - A^l_{41}\theta^l_{,xxxx} - \left(A^l_{44} + A^l_{51} + 2A^l_{62} + 2A^l_{63}\right)\theta^l_{,xxyy}\\
&\quad - A^l_{54}\theta^l_{,yyyy} + \gamma^l_4\theta^l_{,xx} + \gamma^l_5\theta^l_{,yy}\\
P_4 &= A^l_{71}\theta^l_{,xxx} + \left(A^l_{74} + A^l_{82} + A^l_{83}\right)\theta^l_{,xyy} - \left(\gamma^l_7 + \bar{A}^l_{11}\right)\theta^l_{,x}\\
P_5 &= \left(A^l_{92} + A^l_{93} + A^l_{10,1}\right)\theta^l_{,xxy} + A^l_{10,4}\theta^l_{,yyy} - \left(\gamma^l_{10} + \bar{A}^l_{22}\right)\theta^l_{,y}\\
P^j_6 &= -F^j_6 - \left(\bar{A}^{jl}_{31} + \bar{\beta}^{jl}_{11} - \beta^{jl}_1 + \gamma^{jl}_{11}\right)\theta^l_{,xx} - \left(\bar{A}^{jl}_{42} + \bar{\beta}^{jl}_{22}\right.\\
&\quad \left. - \beta^{jl}_4 + \gamma^{jl}_{14}\right)\theta^l_{,yy} + \gamma^{jl}\theta^l + A^{jl}_{11,1}\theta^l_{,xxxx} + \left(A^{jl}_{11,4} + A^{jl}_{12,2}\right.\\
&\quad \left. + A^{jl}_{12,3} + A^{jl}_{13,2} + A^{jl}_{13,3} + A^{jl}_{14,1}\right)\theta^l_{,xxyy} + A^{jl}_{14,4}\theta^l_{,yyyy}
\end{aligned} \tag{29}
$$

To assess the accuracy of the theory developed herein, by comparison with the exact three-dimensional piezothermoelasticity solution,[2,21] an analytical Navier solution is obtained for simply supported rectangular plates of sides a, b along the axes x, y for the boundary conditions

$$
\begin{aligned}
&\text{at } x = 0, \qquad a: N_x, u_{0_y}, w_0, \psi_{0_y}, M_x, P_x, \phi^j, S^j_x = 0\\
&\text{at } y = 0, \qquad b: N_y, u_{0_x}, w_0, \psi_{0_x}, M_y, P_y, \phi^j, S^j_y = 0
\end{aligned} \tag{30}
$$

for $j = 1, \ldots, n_\phi$. The solution is expanded in double Fourier series as

$$
\begin{bmatrix} w_0 & \phi^j \\ p^i_z & \theta^l \\ u_{0_x} & \psi_{0_x} \\ u_{0_y} & \psi_{0_y} \end{bmatrix} = \sum_{n=1}^{\infty}\sum_{m=1}^{\infty} \begin{bmatrix} \left[\left(w_0 \quad \phi^j\right)_{nm}\right] \sin\left(\dfrac{n\pi x}{a}\right) \sin\left(\dfrac{m\pi y}{b}\right) \\ \left[\left(p^i_z \quad \theta^l\right)_{nm}\right] \sin\left(\dfrac{n\pi x}{a}\right) \sin\left(\dfrac{m\pi y}{b}\right) \\ \left[\left(u_{0_x} \quad \psi_{0_x}\right)_{nm}\right] \cos\left(\dfrac{n\pi x}{a}\right) \sin\left(\dfrac{m\pi y}{b}\right) \\ \left[\left(u_{0_y} \quad \psi_{0_y}\right)_{nm}\right] \sin\left(\dfrac{n\pi x}{a}\right) \cos\left(\dfrac{m\pi y}{b}\right) \end{bmatrix} \tag{31}
$$

Substituting these expressions in Eq. (26) yields a system of algebraic equations for n, mth Fourier component

$$
K\bar{U}^{nm} = \bar{P}^{nm} \tag{32}
$$

$\bar{U}$ is partitioned into a set of five mechanical displacement variables U, a set of unknown output voltages Φ_s at z^j_ϕ's where ϕ is not prescribed, and a set of known input actuation voltages Φ_a at the actuated surfaces. $\bar{P}$ is accordingly partitioned into set of five thermomechanical loads P, known input electric loads Q_s and unknown output electrical loads Q_a. Equations (32) are then solved for the unknown variables U and Φ_s. Transverse shear stresses τ and normal stress σ_z are obtained by integrating the three-dimensional equations of equilibrium.

IV. Assessment of the Theory

The accuracy of the present theory is established directly by comparison with the exact three-dimensional piezothermoelasticity solution for simply supported cross-ply hybrid plates. The exact three-dimensional results for the present study have been generated using the solution given by Xu et al.[2] and Kapuria et al.[21] These results will be useful for assessing other approximate theories for hybrid plates under thermal loading, because such elaborate results are scarce in the literature. Because TOT has the same number of displacement variables as the present theory and does not require an arbitrary shear-correction factor, present results are compared with the coupled TOT[12] extended to consider sublayer discretization of thermal and potential fields. To investigate the influence of the thermoelectric transverse normal strain, results are also compared with the particular case of the present theory, referred herein as ZIGT, with uniform w across the thickness obtained by setting $\alpha_3 = 0, d_{33} = 0$. Two simply supported hybrid cross-ply plates a and b, each consisting of an elastic substrate with a piezoelectric layer of PZT-5A of thickness $0.1h$ bonded to its top, are considered for the numerical study. Plate a, which has been devised as a benchmark test case, has a five-ply substrate of thickness $0.09h/0.225h/0.135h/0.18h/0.27h$ of materials 1/2/3/3/3 with the orientation of the principal material direction 1 (in deg) as [0/0/0/90/0]. The plies have very inhomogeneous properties for stiffness in tension and shear and very inhomogeneous coefficients of thermal expansion and thermal conductivities. The substrate of plate b is a graphite–epoxy composite laminate of material 4 with four layers of equal thickness 0.225 h with symmetric layup (in degrees) of [0/90/90/0]. The stacking order is mentioned from the bottom. The PZT-5A layer has poling in $+z$ direction. The top and the bottom of the substrate are grounded. The material properties of materials 1–4 and PZT-5A are[18] as follows:

Material 1:

$$[(Y_L, Y_T, G_{LT}, G_{TT}), \nu_{LT}, \nu_{TT}, (\alpha_L, \alpha_T), (k_L, k_T)]$$
$$= [(6.9, 6.9, 1.38, 1.38)\ \text{GPa}, 0.25, 0.25, (35.6, 35.6) \times 10^{-6}\ \text{K}^{-1}, (0.12, 0.12)\ \text{Wm}^{-1}\text{K}^{-1}]$$

Material 2:

$$[(Y_L, Y_T, G_{LT}, G_{TT}), \nu_{LT}, \nu_{TT}, (\alpha_L, \alpha_T), (k_L, k_T)]$$
$$= [(224.25, 6.9, 56.58, 1.38)\ \text{GPa}, 0.25, 0.25, (0.25, 35.6) \times 10^{-6}\ \text{K}^{-1}, (7.2, 1.44)\ \text{Wm}^{-1}\text{K}^{-1}]$$

Material 3:

$$[(Y_L, Y_T, G_{LT}, G_{TT}), \nu_{LT}, \nu_{TT}, (\alpha_L, \alpha_T), (k_L, k_T)]$$
$$= [(172.5, 6.9, 3.45, 1.38)\ \text{GPa}, 0.25, 0.25, (0.57, 35.6) \times 10^{-6}\ \text{K}^{-1}, (1.92, 0.96)\ \text{Wm}^{-1}\text{K}^{-1}]$$

Material 4:

$$[(Y_L, Y_T, G_{LT}, G_{TT}), \nu_{LT}, \nu_{TT}, (\alpha_L, \alpha_T), (k_L, k_T)]$$
$$= [(181, 10.3, 7.17, 2.87)\ \text{GPa}, 0.28, 0.33, (0.02, 22.5) \times 10^{-6}\ \text{K}^{-1}, (1.5, 0.5)\ \text{Wm}^{-1}\text{K}^{-1}]$$

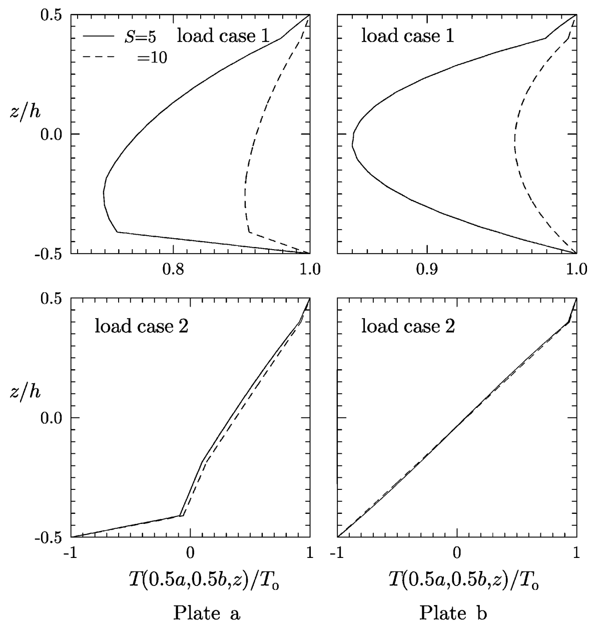

Fig. 2 Temperature distributions in square plates a and b.

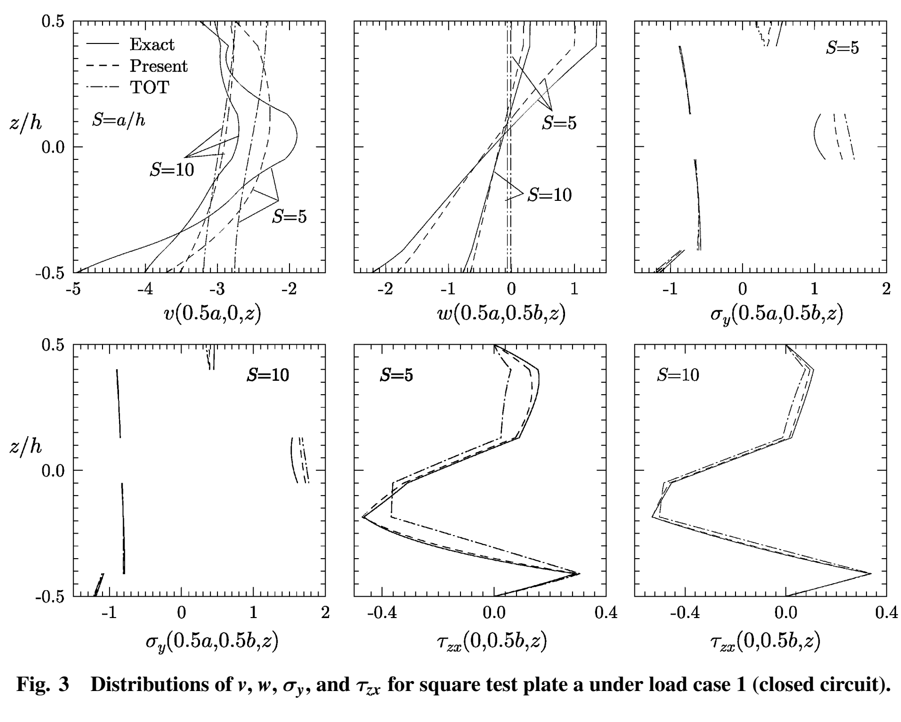

Fig. 3 Distributions of v, w, σ_y, and τ_{zx} for square test plate a under load case 1 (closed circuit).

PZT-5A:

$[(Y_1, Y_2, Y_3, G_{12}, G_{23}, G_{31}), \nu_{12}, \nu_{13}, \nu_{23}]$

$= [(61.0, 61.0, 53.2, 22.6, 21.1, 21.1)$ GPa, 0.35, 0.38, 0.38]

$[(d_{31}, d_{32}, d_{33}, d_{15}, d_{24}), (\eta_{11}, \eta_{22}, \eta_{33})]$

$= [(-171, -171, 374, 584, 584) \times 10^{-12}$ m/V,

$(1.53, 1.53, 1.5) \times 10^{-8}$ F/m]

$[(\alpha_1, \alpha_2, \alpha_3), k_i, p_3] = [(1.5, 1.5, 2.0) \times 10^{-6}\ \mathrm{K}^{-1}$,

$1.8\ \mathrm{Wm^{-1}K^{-1}}, 0.0007\ \mathrm{Cm^{-2}K^{-1}}]$

where L and T denote directions parallel and transverse to the fibers, ν_{LT} is Poisson's ratio for strain in the T direction under uniaxial normal stress in the L direction, and k_L, k_T, k_i are the thermal conductivity coefficients.

Two load cases are considered, which consist of equal temperature rise at $z = \pm h/2$ and equal temperature rise and fall at $z = \pm h/2$ with sinusoidal inplane variations:

1) $\theta(x, y, \pm h/2) = T_0 \sin(\pi x/a) \sin(\pi y/b)$,

2) $\theta(x, y, h/2) = -\theta(x, y, -h/2) = T_0 \sin(\pi x/a) \sin(\pi y/b)$, with open or closed circuit conditions at the top surface.

The three-dimensional thermal problem is solved by exact analytical solution of the heat conduction equation for all the layers and exact satisfaction of the thermal boundary conditions at the top, bottom, and four sides, and the continuity conditions at the layer interfaces for temperature and heat flow. The distributions of temperature across the thickness for the two load cases are shown in Fig. 2. The test plate a, devised for this study, has a highly nonlinear temperature distribution across the thickness with large discontinuities in its slope and hence is a good case for assessing two-dimensional theories. Convergence studies have revealed that converged results are obtained by dividing each layer into four equal sublayers for the temperature discretization and

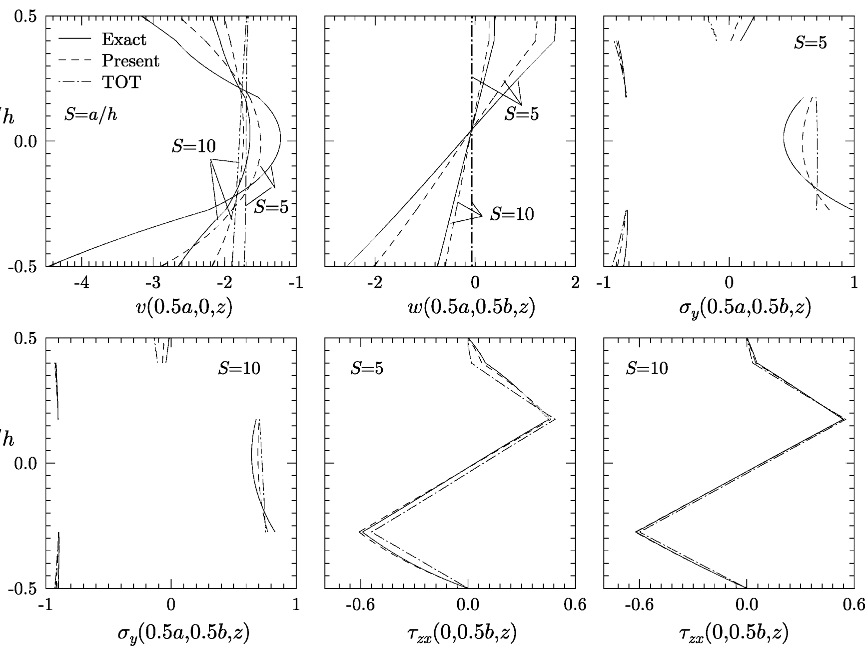

Fig. 4 Distributions of v, w, σ_y, and τ_{zx} for square composite plate b under load case 1 (closed circuit).

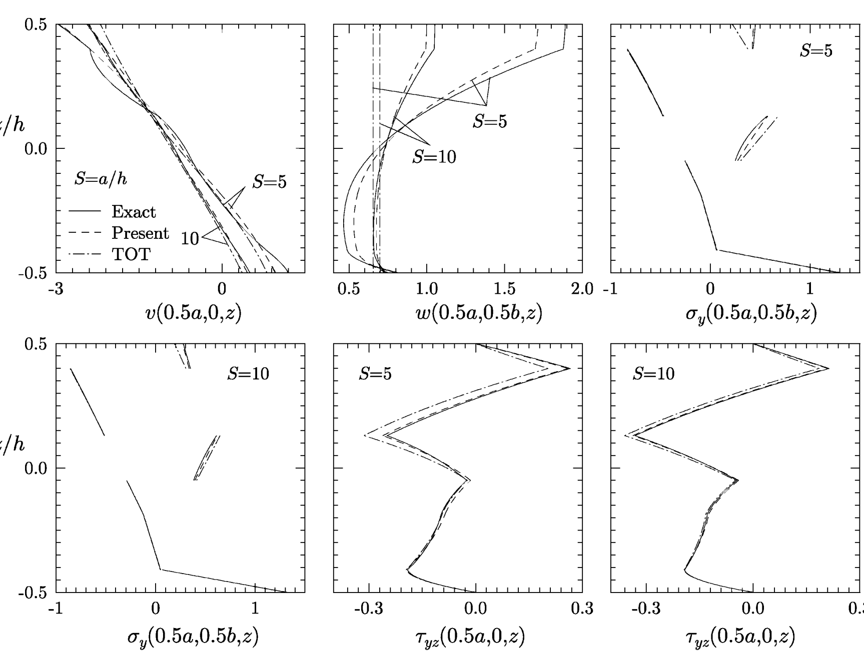

Fig. 5 Distributions of v, w, σ_y, and τ_{yz} for square test plate a under load case 2 (closed circuit).

dividing the piezoelectric layer into four sublayers for the potential discretization.

The results for these cases are nondimensionalized with the respective values of Y_T and α_T for plates a and b and $d_T = 374 \times 10^{-12}$ CN^{-1}. S is the span-to-thickness ratio a/h:

$$(\bar{u}, \bar{v}, \bar{w}) = 100(u_x, u_y, w/S)/\alpha_T S h T_0$$

$$(\bar{\sigma}_x, \bar{\sigma}_y, \bar{\tau}_{xy}) = (\sigma_x, \sigma_y, \tau_{xy})/\alpha_T Y_T T_0$$

$$(\bar{\tau}_{yz}, \bar{\tau}_{zx}, \bar{\sigma}_z) = (\tau_{yz}, \tau_{zx}, S\sigma_z)S/\alpha_T Y_T T_0$$

$$\bar{\phi} = 10\phi d_T/\alpha_T h T_0, \qquad \bar{D}_z = D_z/Y_T \alpha_T d_T T_0$$

The dimensionless entities are chosen in such a way that their values are almost independent of S for thin plates that have large values of S. The overbar is omitted in the following discussion for simplicity.

The thickness distributions of deflection w, predominant in-plane displacement v, in-plane stress σ_y and transverse shear stress τ_{zx} or τ_{yz}, obtained by the present theory for square plates, are compared in Figs. 3–6 with the exact three-dimensional thermopiezoelasticity solution and the coupled TOT solution. Results are compared in Figs. 3 and 4 for load case 1 and in Figs. 5 and 6 for load case 2, with closed-circuit condition at the top surface $[\phi(x, y, h/2) = \phi^{n_\phi} = 0]$ for thick ($S = 5$) and moderately thick ($S = 10$) plates a and b. It is observed that the nonuniform distributions of w obtained from the present theory are in good qualitative agreement with the exact three-dimensional solution for both plates with $S = 5$ and 10 for both load cases, with a quantitative error, which is small for $S = 10$, whereas the uniform distributions of w for TOT are very erroneous. The σ_y distributions for the present theory are much superior to those for TOT, which yields very erroneous distribution in the elastic layers with material axis 1 at 90 deg and the PZT layer. The distributions of postprocessed τ_{zx}/τ_{yz} obtained by the present theory closely follow the exact three-dimensional solution for all cases, whereas TOT yields inaccurate distributions for plate a. The v distributions of the zigzag theory, even though far superior to those of TOT, deviate from the three-dimensional solution, particularly for load case 1, with reversal of curvature in some layers. It appears from the results

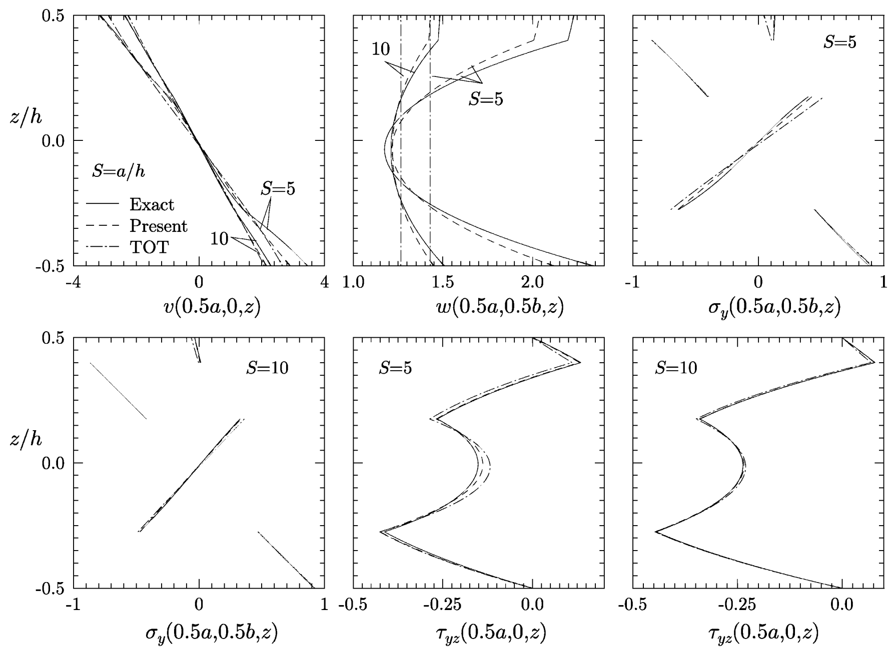

Fig. 6 Distributions of u, w, σ_y, and τ_{yz} for square composite plate b under load case 2 (closed circuit).

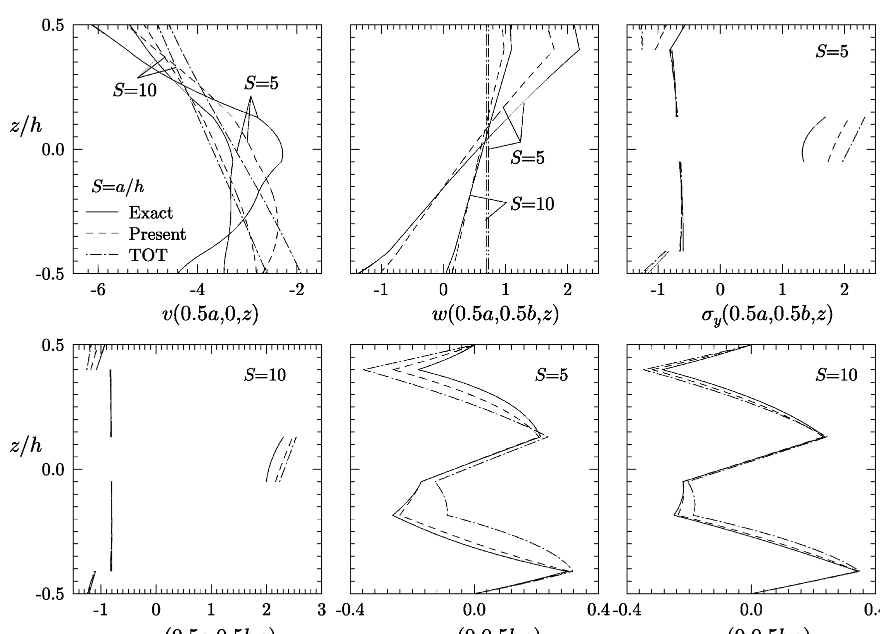

Fig. 7 Distributions of v, w, σ_y, and τ_{yz} for square test plate a under load case 1 (open circuit).

Table 1 Exact results and percent error of present theory, ZIGT, and TOT for square test plate a

		Load case 1					Load case 2			
S	Entity	Exact	Present	ZIGT	TOT	Entity	Exact	Present	ZIGT	TOT
5	$w(-0.5h)$	−2.21736	−17.65	−87.86	−99.46	$w(0.5h)$	1.88946	−9.06	−52.68	−65.29
10		−0.77073	−15.16	−78.69	−91.37		1.05161	−5.00	−25.61	−33.69
20		−0.28390	−10.96	−57.03	−67.06		0.80429	−1.75	−8.59	−11.58
40		−0.15022	−5.27	− 27.42	−32.36		0.73859	−0.49	−2.36	−3.20
5	$\sigma_y(-0.05h^+)$	1.14790	20.62	35.66	35.13	$\sigma_y(0.13h^-)$	0.57106	0.86	8.32	19.27
10		1.61473	6.69	10.03	9.61		0.61167	1.02	2.98	5.68
20		1.79131	1.79	2.59	2.44		0.62444	0.31	0.81	1.44
40		1.84078	0.45	0.65	0.61		0.62759	0.08	0.20	0.36
5	$\sigma_y(0.5h)$	0.55330	−29.09	−74.22	−67.03	$\sigma_y(0.4h^+)$	0.42723	−1.67	−3.76	−12.16
10		0.45663	−15.32	−32.03	−25.33		0.34919	−3.78	−3.04	−13.08
20		0.43179	−4.60	−9.32	−6.83		0.30030	−3.51	−3.41	−7.11
40		0.42678	−1.11	−2.33	−1.64		0.28451	−3.29	−3.27	−4.31
5	$\tau_{zx}(-0.185h)$	−0.46558	1.32	−19.94	−20.96	$\tau_{yz}(0.13h)$	−0.24913	4.81	12.29	26.12
10		−0.53162	−0.29	−6.27	−5.60		−0.33182	1.74	3.71	8.90
20		−0.55957	−0.11	−1.64	−1.33		− 0.36793	0.48	0.98	2.45
40		−0.56814	−0.03	−0.41	−0.32		−0.37878	0.13	0.25	0.63
5	$\tau_{xy}(0.5h)$	−0.45651	−12.62	−37.21	−34.01	$\tau_{xy}(0.5h)$	−0.46666	−3.10	−14.02	−20.49
10		−0.38642	−6.47	−15.15	−12.73		−0.40113	−1.65	−5.26	−8.57
20		−0.36375	−1.99	−4.43	−3.56		−0.37449	−0.53	−1.54	−2.62
40		−0.35792	−0.53	−1.15	−0.91		−0.36664	−0.15	−0.41	−0.70
5	$D_z(0.5h)$	7.27127	1.66	3.79	3.57	$D_z(0.5h)$	7.09337	1.21	2.05	2.71
10		7.46748	0.70	1.34	1.16		7.22643	1.01	1.25	1.55
20		7.53217	0.22	0.38	0.32		7.27858	0.89	0.96	1.05
40		7.54924	0.07	0.11	0.10		7.29377	0.86	0.88	0.90

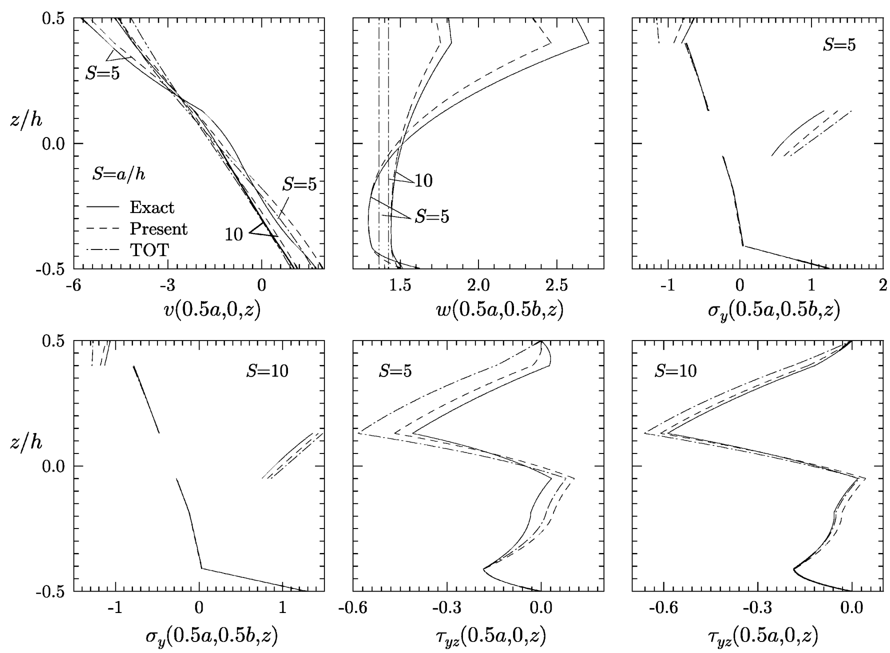

Fig. 8 Distributions of v, w, σ_y, and τ_{yz} for square test plate a under load case 2 (open circuit).

that the global quadratic terms in u and v predominate and distort the local distributions in some layers. The pattern of the distributions of u/v for the exact solution suggests that the present zigzag model may be improved by replacing the global quadratic term by a layerwise quadratic term in the approximation of u and v. This would require a separate study. The results for square plate a with open-circuit condition $[D_z(x, y, h/2) = 0]$ at the top are presented in Figs. 7 and 8 for load cases 1 and 2, respectively. For this case too, the present theory yields quite accurate distributions of w, σ_y, τ_{zx}/τ_{yz} for moderately thick plates. Comparison of these distributions with those for the closed-circuit condition in Figs. 3 and 5 reveals that the electrical boundary conditions have a large effect on both the magnitude and the nature of the distribution of v, σ_y, τ_{yz}/τ_{zx} for both load cases and on the magnitude of w. A large potential is induced at the top surface because of the presence of pyroelectric coupling to satisfy the open-circuit condition $D_z = 0$. Consequently, the displacements and stresses in the open-circuit condition differ significantly from those for the closed-circuit condition.

The exact three-dimensional results for displacements, stresses, and D_z at typical points across the thickness, where they are large, along with the percent errors in the present theory, ZIGT, and coupled TOT, are given in Tables 1 and 2 for plates a and b under two load cases with closed circuit condition for $S = 5$, 10, 20, and 40. The errors in the TOT for w are large and the ZIGT is only a marginal improvement over TOT. Even for thin plates a and b with $S = 20$, the errors in w for TOT are as large as 67.1, 67.1% for load case 1 and 11.6, 4.9% for load case 2, respectively. The corresponding errors in w for the present theory are 11.0, 15.3% and 1.8, 1.2% for load cases 1 and 2, respectively. The errors in w for ZIGT are only marginally smaller than TOT, being 57.1, 64.9% for load case 1 and

Table 2 Exact results and percent error of present theory, ZIGT, and TOT for square composite plate b

		Load case 1					Load case 2			
S	Entity	Exact	Present	ZIGT	TOT	Entity	Exact	Present	ZIGT	TOT
5	$w(-0.5h)$	−2.56626	−21.26	−93.91	−98.09	$w(-0.5h)$	2.34089	−9.48	−37.53	−38.92
10		−0.75216	−20.27	−86.88	−90.00		1.50806	−3.94	−15.07	−16.06
20		−0.25669	−15.25	−64.88	−67.01		1.26431	−1.21	−4.55	−4.91
40		−0.13045	−7.55	−32.06	−33.09		1.19983	−0.33	−1.21	−1.31
5	$\sigma_y(-0.5h)$	−0.84308	5.78	10.86	10.88	$\sigma_y(-0.275h^+)$	−0.63523	0.81	1.42	9.79
10		−0.90259	1.63	2.84	2.81		−0.47182	−0.24	−0.11	2.96
20		−0.91940	0.42	0.72	0.71		−0.40262	−0.16	−0.13	0.76
40		−0.92370	0.11	0.18	0.18		−0.38236	−0.06	−0.05	0.18
5	$\sigma_x(0.4h^+)$	−0.06877	18.42	78.72	84.16	$\sigma_x(0.5h)$	−0.03920	97.28	198.7	264.6
10		−0.09867	6.93	18.28	19.32		−0.09954	7.94	18.28	27.53
20		−0.10956	2.03	4.63	4.87		−0.11985	−1.71	0.46	2.60
40		−0.11256	0.72	1.35	1.41		−0.12543	−3.79	−3.28	−2.75
5	$\tau_{zx}(-0.275h)$	−0.59014	3.26	−5.66	−8.59	$\tau_{yz}(-0.275h)$	−0.41307	2.89	4.16	3.22
10		−0.62022	0.69	−2.21	−3.23		−0.44420	0.70	1.01	0.77
20		−0.62244	0.16	−0.64	−0.93		−0.45393	0.18	0.25	0.19
40		−0.62235	0.04	−0.17	−0.24		−0.45656	0.04	0.06	0.05
5	$\tau_{xy}(0.5h)$	−0.35661	−11.11	−36.47	−38.84	$\tau_{xy}(0.5h)$	−0.34997	−3.66	−7.71	−12.74
10		−0.27240	−4.93	−14.57	−15.74		−0.29475	−1.41	−2.66	−5.00
20		−0.24390	−1.50	−4.32	−4.69		−0.27405	−0.42	−0.76	−1.49
40		−0.23610	−0.39	−1.13	−1.23		−0.26817	−0.11	−0.20	−0.39
5	$D_z(0.5h)$	8.02271	0.91	2.53	2.77	$D_z(0.5h)$	7.85080	0.94	1.07	1.48
10		8.20368	0.31	0.78	0.86		7.95928	0.75	0.78	0.94
20		8.26271	0.09	0.21	0.24		7.99806	0.69	0.70	0.74
40		8.27869	0.03	0.06	0.07		8.00895	0.67	0.67	0.68

Table 3 Exact results and percent error of present theory, ZIGT, and TOT for rectangular plate a ($b/a = 1.5$)

		Load case 1					Load case 2			
S	Entity	Exact	Present	ZIGT	TOT	Entity	Exact	Present	ZIGT	TOT
5	$w(0.5h)$	1.57364	−19.59	−104.86	−96.05	$w(0.5h)$	2.01016	−9.27	−52.03	−64.62
10		0.46256	−19.40	−98.18	−88.60		1.10615	−4.94	−25.08	−32.88
20		0.15055	−15.44	−77.44	−69.36		0.84790	−1.70	−8.34	−11.15
40		0.07030	−8.33	−41.74	−37.30		0.78026	−0.48	−2.29	−3.07
5	$\sigma_y(-0.05h^+)$	0.79084	10.65	24.46	24.29	$\sigma_y(0.13h^-)$	0.38352	−3.00	2.94	16.28
10		1.03457	3.50	6.65	6.57		0.36993	−1.60	0.05	3.79
20		1.12137	0.94	1.70	1.68		0.35872	−0.54	−0.11	0.84
40		1.14538	0.24	0.43	0.42		0.35490	−0.15	−0.04	0.20
5	$\tau_{zx}(-0.185h)$	−0.34377	1.82	−23.10	−24.56	$\tau_{yz}(0.13h)$	0.19520	2.18	8.12	18.53
10		−0.35193	0.02	−7.42	−7.65		0.25210	0.78	2.27	5.92
20		−0.35461	−0.03	−1.98	−2.02		0.27458	0.22	0.59	1.60
40		−0.35542	−0.01	−0.50	−0.51		0.28108	0.06	0.15	0.41
5	$\tau_{xy}(0.5h)$	−0.46704	−5.74	−22.54	−21.52	$\tau_{xy}(0.5h)$	0.41493	−1.94	−10.86	−18.36
10		−0.43122	−2.29	−7.62	−6.88		0.34404	−0.97	−4.02	−7.83
20		−0.42182	−0.64	−2.07	−1.82		0.31664	−0.32	−1.18	−2.40
40		−0.41959	−0.16	−0.53	−0.46		0.30876	−0.09	−0.31	−0.64
5	$D_z(0.5h)$	7.39673	0.78	2.44	2.37	$D_z(0.5h)$	7.24823	1.19	1.93	2.41
10		7.54943	0.27	0.74	0.70		7.36915	0.99	1.19	1.38
20		7.59609	0.07	0.19	0.18		7.41135	0.90	0.95	1.01
40		7.60830	0.01	0.04	0.04		7.42312	0.88	0.89	0.90

8.6, 4.6% for load case 2 for plates a and b, respectively. For the moderately thick plate with $S = 10$, the maximum error in w for the present theory is 5.0% for load case 2, whereas the corresponding errors for TOT and ZIGT are 33.7 and 25.6%, respectively.

A comparison of the results for σ_y in elastic layers reveals that the percent error in the present theory is much smaller compared to the TOT for all cases with the errors being even one order less for load case 2. The percent error in the predominant in-plane stress σ_x/σ_y in the piezoelectric layer is also significantly less for the present theory compared to the TOT for all cases except for a marginal increase in error in the present theory for plate b with $S = 40$ under load case 2, because $S = 40$ is in the transition zone for a change in the sign of error. The present theory yields very accurate results for the postprocessed τ_{yz}/τ_{zx}. The maximum error in τ_{yz}/τ_{zx} for the present theory for moderately thick plates ($S = 10$) is 1.7%, whereas the corresponding error for TOT is 8.9%. For in-plane shear τ_{xy} and the transverse electric displacement D_z, too, there is significant reduction of error in the present theory compared to the TOT. The results of ZIGT for the stresses and D_z, for both load cases are either a small improvement or a small deterioration over those of TOT, except for σ_y in the elastic layers for both plates and in the PZT layer for plate a under load case 2, where ZIGT shows moderate improvement over TOT.

The results of rectangular hybrid plate a with $b/a = 1.5$ are presented in Table 3. It is observed by comparing Tables 1 and 3 that there is marginal reduction in the error for stresses for both load cases for $b/a = 1.5$ except for a marginal increase in error for τ_{zx} for load case 1. The errors in w for $b/a = 1.5$ for the present theory and TOT are marginally less than that for $b/a = 1$ for both loads.

The distributions of the postprocessed transverse normal stress σ_z obtained from the present theory, ZIGT, and TOT for load cases 1 and 2 are compared with the three-dimensional exact solution for square plates a and b in Figs. 9 and 10 for $S = 5$ and 10, respectively. The present theory yields consistently superior results compared to TOT and ZIGT for all cases. The distributions in the present theory are in good qualitative agreement and fair quantitative agreement with the three-dimensional solution. In contrast, the TOT and ZIGT predictions are very poor, particularly for load case 1.

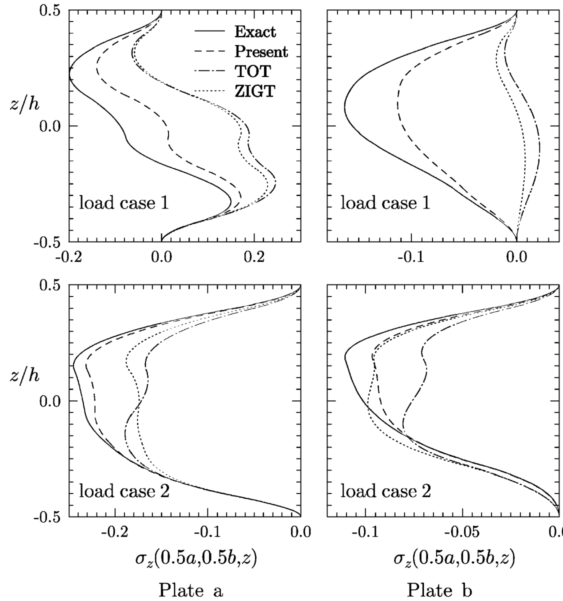

Fig. 9 Distributions of σ_z for thick square plates ($S = 5$).

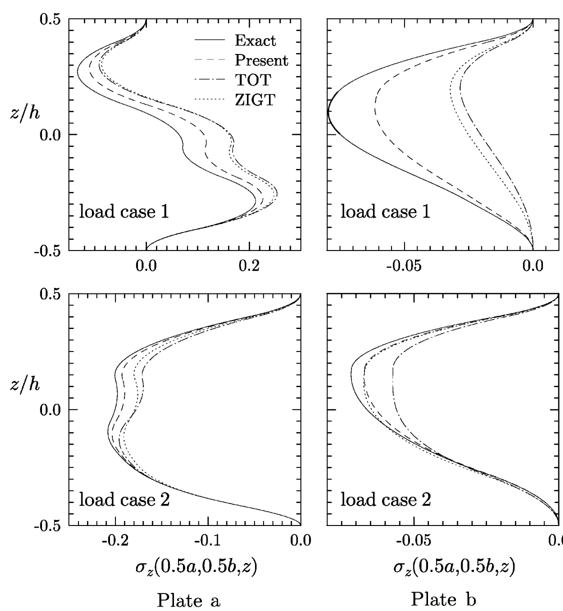

Fig. 10 Distributions of σ_z for moderately thick plates ($S = 10$).

V. Conclusions

An efficient electromechanically coupled ZIGT has been developed for hybrid piezoelectric plates under thermoelectric loading in terms of five displacement variables, which accounts for the nonuniform deflection across the thickness resulting from the transverse normal strain caused by the thermal and thermal fields without introducing any additional displacement variables and satisfies exactly the conditions on transverse shear stress at the top, bottom, and layer interfaces for the case of nonzero in-plane electric fields. The present theory can effectively model closed-circuit as well as open-circuit electric boundary conditions in the piezoelectric layer as required in sensory and active applications. The accuracy of the theory is established directly by comparison with the exact three-dimensional piezothermoelasticity solutions for two thermal loads on a hybrid test plate devised for this study and a hybrid composite plate, with different aspect ratios for both open-circuit and closed-circuit boundary conditions. The present theory generally yields quite accurate results for all entities including the nonuniform variation of w and σ_z for moderately thick plates. The theory is as efficient as coupled TOT, because both have exactly the same number of primary displacement and potential variables. Yet, it is much more accurate than TOT and also ZIGT with uniform w across the thickness. The results of TOT and ZIGT generally do not show any significant difference for thermal loads. The theory is applicable without change to hybrid piezoelectric sandwich plates.

Acknowledgment

This work was supported by the Department of Science and Technology, Government of India, through a financial grant in the Science and Engineering Research Council scheme.

References

[1]Tauchert, T. R., Ashida, F., Noda, N., and Verijenko, V., "Developments in Thermopiezoelasticity with Relevance to Smart Composite Structures," *Composite Structures*, Vol. 48, No. 1–3, 2000, pp. 31–45.

[2]Xu, K., Noor, A. K., and Tang, Y. Y., "Three-Dimensional Solutions for Coupled Thermoelectroelastic Response of Multilayered Plates," *Computer Methods in Applied Mechanics and Engineering*, Vol. 126, No. 3–4, 1995, pp. 355–371.

[3]Tauchert, T. R., "Piezothermoelastic Behavior of a Laminated Plate," *Journal of Thermal Stresses*, Vol. 15, No. 1, 1992, pp. 25–37.

[4]Rao, S. S., and Sunar, M., "Analysis of Distributed Thermopiezoelectric Sensors and Actuators in Advanced Intelligent Structures," *AIAA Journal*, Vol. 31, No. 7, 1993, pp. 1280–1286.

[5]Jonnalagadda, K. D., Blandford, G. E., and Tauchert, T. R., "Piezothermoelastic Composite Plate Analysis Using First-Order Shear Deformation Theory," *Computers and Structures*, Vol. 51, No. 1, 1994, pp. 79–89.

[6]Kapuria, S., Dube, G. P., Dumir, P. C., and Sengupta, S., "Levy-Type Piezothermoelastic Solution for Hybrid Plate Using First-Order Shear Deformation Theory," *Composites Part B: Engineering*, Vol. 28, No. 5–6, 1997, pp. 535–546.

[7]Ishiara, M., and Noda, N., "Piezothermoelastic Analysis of a Cross-Ply Laminate Considering the Effects of Transverse Shear and Coupling," *Journal of Thermal Stresses*, Vol. 23, No. 5, 2000, pp. 441–461.

[8]Kapuria, S., and Dumir, P. C., "Coupled FSDT for Piezothermoelectric Hybrid Rectangular Plate," *International Journal of Solids and Structures*, Vol. 37, No. 42, 2000, pp. 6131–6153.

[9]Krommer, V. M., and Irschik, H., "A Reissner–Mindlin Type Plate Theory Including the Direct Piezoelectric and the Pyroelectric Effect," *Acta Mechanica*, Vol. 141, No. 1–2, 2000, pp. 51–69.

[10]Shen, S., and Kuang, Z. B., "An Active Control Model of Laminated Piezothermoelastic Plate," *International Journal of Solids and Structures*, Vol. 36, No. 13, 1999, pp. 1925–1947.

[11]Gu, H., Chattopadhyay, A., Li, J., and Zhou, C., "A Higher Order Temperature Theory for Coupled Thermo-Piezoelectro-Mechanical Modelling of Smart Structures," *International Journal of Solids and Structures*, Vol. 37, No. 44, 2002, pp. 6479–6497.

[12]Zhou, X., Chattopadhyay, A., and Gu, H., "Dynamic Responses of Smart Composite Using a Coupled Thermo-Piezoelectric-Mechanical Model," *AIAA Journal*, Vol. 38, No. 10, 2000, pp. 1939–1948.

[13]Tang, Y. Y., Noor, A. K., and Xu, K., "Assessment of Computational Models for Thermoelectroelastic Multilayered Plates," *Computers and Structures*, Vol. 61, No. 5, 1996, pp. 915–933.

[14]Kim, H. S., Xu, Z., and Chattopadhya, A., "Interlaminar Stress Analysis of Shell Structures with Piezoelectric Patch Including Thermal Loading," *AIAA Journal*, Vol. 40, No. 12, 2002, pp. 2517–2525.

[15]Cho, M., and Oh, J., "Higher Order Zigzag Theory for Fully Coupled Thermo-Electro-Mechanical Smart Composite Plates," *International Journal of Solids and Structures*, Vol. 41, No. 5–6, 2004, pp. 1331–1356.

[16]Yang, J. S., "Equations for Thick Elastic Plates with Partially Electroded Piezoelectric Actuators and Higher Order Electric Field," *Smart Materials and Structures*, Vol. 8, No. 1, 1999, pp. 73–82.

[17]Carrera, E., "Temperature Profile Influence on Layered Plates Response Considering Classical and Advanced Theories," *AIAA Journal*, Vol. 40, No. 9, 2002, pp. 1885–1896.

[18]Kapuria, S., Ahmed, A., and Dumir, P. C., "Efficient Coupled Zigzag Theory for Hybrid Piezoelectric Beams for Thermoelectric Load," *AIAA Journal*, Vol. 42, No. 2, 2004, pp. 383–394.

[19]Kapuria, S., "A Coupled Zigzag Third Order Theory for Hybrid Cross-Ply Plates," *Journal of Applied Mechanics*, Vol. 71, No. 5, 2004, pp. 604–614.

[20]Kapuria, S., and Achary, G. G. S., "An Efficient Higher Order Zigzag Theory for Laminated Plates Subjected to Thermal Loading," *International Journal of Solids and Structures*, Vol. 41, No. 16–17, 2004, pp. 4661–4684.

[21]Kapuria, S., Dumir, P. C., and Sengupta, S., "Three-Dimensional Solution for Shape Control of Rectangular Hybrid Plate," *Journal of Thermal Stresses*, Vol. 22, No. 2, 1999, pp. 159–176.

[22]Tiersten, H. F., *Linear Piezoelectric Plate Vibrations*, Plenum, New York, 1969, pp. 25, 37, 54, 55.

K. Shivakumar
Associate Editor